ACS APPLIED MATERIALS & INTERFACES

Research Article

www.acsami.org

Optimized Carbonation of Magnesium Silicate Mineral for CO_2 Storage

Espen Eikeland,[†] Anders Bank Blichfeld,[†] Christoffer Tyrsted,[†] Anca Jensen,[‡] and Bo Brummerstedt Iversen*[,†]

[†]Center for Materials Crystallography, Department of Chemistry and iNANO, Aarhus University, DK-8000 Aarhus C, Denmark

[‡]FLSmidth A/S, Valby, Denmark

Supporting Information

ABSTRACT: The global ambition of reducing the carbon dioxide emission makes sequestration reactions attractive as an option of storing CO_2. One promising environmentally benign technology is based on forming thermodynamically stable carbonated minerals, with the drawback that these reactions usually have low conversion rates. In this work, the carbonation reaction of Mg rich olivine, Mg_2SiO_4, under supercritical conditions has been studied. The reaction produces $MgCO_3$ at elevated temperature and pressure, with the addition of $NaHCO_3$ and NaCl to improve the reaction rates. A sequestration rate of 70% was achieved within 2 h, using olivine particles of sub-10 μm, whereas 100% conversion was achieved in 4 h. This is one of the fastest complete conversions for this reaction reported to date. The CO_2 sequestration rate is found to be highly dependent on the applied temperature and pressure, as well as the addition of $NaHCO_3$. In contrast, adding NaCl was found to have limited effect on the reaction rate. The roles of $NaHCO_3$ and NaCl as catalysts are discussed and especially how their effect changes with increased olivine particle size. The products have been characterized by Rietveld refinement of powder X-ray diffraction, scanning electron microscopy (SEM), and energy-dispersive X-ray (EDX) spectroscopy revealing the formation of amorphous silica and micrometer-sized magnesium carbonate crystals.

$$Mg_2SiO_4(s) + 2CO_2(g) \xrightarrow{p,T,t,\ NaHCO_3,\ NaCl} 2MgCO_3(s) + SiO_2(s)$$

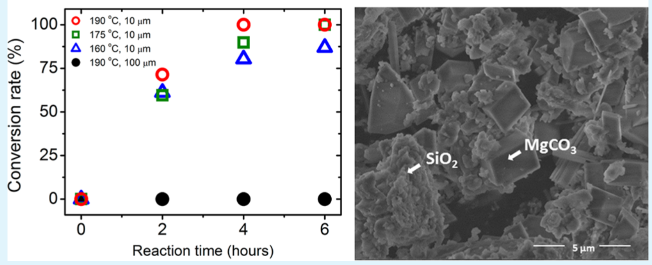

KEYWORDS: *CO_2 capture, storage and utilization, CSU, sequestration, carbonation, reducing CO_2 emission, magnesium silicates*

■ INTRODUCTION

Atmospheric CO_2 levels are increasing, and at a progressively faster rate each decade since the industrial revolution. Even with a stable global CO_2 emission in the next decades, the atmospheric concentration will have doubled by 2050, compared with the preindustrial CO_2 level of ca. 280 ppm.[1−3] Despite recent advances in renewable energy sources, e.g., solar and wind power, fossil fuels will remain the dominating energy source in the coming decades, at present responsible for more than 70% of anthropogenic CO_2 emission.[4] The predicted environmental impact of elevated atmospheric CO_2 levels has in recent years resulted in worldwide efforts in developing new technologies for CO_2 capture, storage, and utilization (CSU).[5−7] The majority of new technologies are based on either physical or chemical adsorption. Physical adsorbents in general, e.g., zeolites, are porous and have high surface areas, and materials such as MOFs and carbon-based compounds also have high gas selectivity with tunable pore size and chemical functionalization.[5,8−10] Their main disadvantage is low thermal, chemical, and mechanical stabilities, and as a result they are not ideal as permanent storage materials. CO_2 sequestration by chemical adsorption (often carbonation) on the other hand binds the gas molecules and is therefore more stable. A number of these compounds have been studied including $Mg_3Si_2O_5(OH)_4$, $CaSiO_3$, Li_2ZrO_3, and CaO,[11−15] where the last two materials are important as high-temperature solid adsorbents (>400 °C).[5] For permanent large scale CO_2 storage a cheap, and readily available mineral would be desirable. Mineral carbonation mimics the natural process of mineral weathering and is one of the safest, permanent alternatives for CO_2 storage, with the general drawback of slow reaction rates.[16] The most abundant minerals with carbonation potential are the magnesium silicates, where olivine (Mg_2SiO_4) has been found to have improved reaction kinetics compared to serpentine ($Mg_3Si_2O_5(OH)_4$).[17] The chemical formulas are here idealized since naturally occurring magnesium silicates often contains Ca^{2+} and Fe^{2+} impurities. Overall carbonation of olivine is promising owing to its worldwide availability, reflected in the low price of 4−5 \$/ton,[18] its reactivity[19] and exothermic carbonation (**1**) along with its high sequestration potential of ca. 0.6 ton CO_2 per. ton of Mg_2SiO_4.[20−27] Furthermore, the reaction is also of interest to

Received: December 3, 2014
Accepted: February 17, 2015
Published: February 17, 2015

   DOI: 10.1021/am508432w
ACS Appl. Mater. Interfaces 2015, 7, 5258−5264

cement manufactures, because the end product of olivine carbonation is magnesium carbonate ($MgCO_3$), found in limestone. CO_2 released during limestone calcination may be captured and recycled by silicate mineral carbonation earlier in the process, producing additional limestone.[3]

The hydrothermal model proposed for carbonation of the Mg-rich olivine end-member, forsterite, is described schematically as[28,29]

$$Mg_2SiO_4(s) + 2CO_2(g) \xrightarrow{p,T,t,H_2O,NaHCO_3,NaCl} 2MgCO_3(s) + SiO_2(s) \quad (1)$$

Where p, T, and t are pressure, temperature and reaction time, respectively. The model implies injection of CO_2 and water under elevated levels of temperature and pressure. Previous results have shown that the degree of carbonation is sensitive not only to the CO_2 conditions but also to the presence of water.[30,31] The CO_2 is dissolved in water to form carbonic acid according to the following equilibria:[3]

$$CO_2(g) + H_2O(l) \overset{(2)}{\leftrightarrow} H_2CO_3(aq) \overset{(3)}{\leftrightarrow} H^+(aq) + HCO_3^-(aq) \overset{(4)}{\leftrightarrow} 2H^+(aq) + CO_3^{2-}(aq)$$

The acid reacts with the olivine releasing Mg^{2+} ions, which further reacts with carbonate ions forming magnesite

$$Mg_2SiO_4(s) + 4H^+(aq) \rightarrow 2Mg^{2+}(aq) + H_4SiO_4(aq) \quad (5)$$

$$Mg^{2+}(aq) + CO_3^{2-}(aq) \leftrightarrow MgCO_3(s) \quad (6)$$

High, or supercritical, CO_2 pressures ensure that carbonic acid is continuously generated when consumed by the reaction above. O'Connor et al. found that addition of $NaHCO_3$ and NaCl to the process leads to a significant increase in sequestration rates, although the individual roles of the additives were not well established.[30] To remedy this the effect of both additives are investigated separately in the present study, together with how reaction time, temperature and pressure influences the conversion of smaller, <10 μm, and bigger, ~100 μm, olivine particles. Our study concludes with a thorough comparison with earlier work, discussing the role of NaCl and $NaHCO_3$ and how they are affected by the size of the olivine particles.

All products have been characterized by powder X-ray diffraction (PXRD) with carbonation rates determined by quantitative phase analysis using Rietveld refinement. The elemental composition of selected reaction products were determined by scanning electron microscopy (SEM) and simultaneous energy-dispersive X-ray (EDX) analysis. The size distributions of the two different olivine samples were determined by SEM.

EXPERIMENTAL SECTION

Synthesis. NaCl (>99%, Sigma-Aldrich) and $NaHCO_3$ (>99%, Sigma-Aldrich) were used without further purification. The Mg rich olivine/forsterite (Mg_2SiO_4) sample was provided by SIBELCO and originating from their Åheim Plant, Norway, and ground to particle sizes of <10 μm and ~100 μm. Two grams of olivine were mixed with 10 mL water and different amounts of NaCl and $NaHCO_3$ to form a slurry. The slurry was then transferred, along with a stirring magnet to an in-house designed Teflon lined autoclave. In all experiments the stirring rate was set to 1500 rpm. Figure 1 shows a flow diagram over the specially designed setup used to heat and pressurize the autoclave. The majority of experiments were conducted at conditions above the critical point of pure CO_2 (P_{crit} = 73 bar, T_{crit} = 31 °C). When the desired synthesis durations were reached, the autoclave was cooled in water baths to rapidly stop the reaction. Thereby, a clear duration of synthesis was determined. The products were subsequently dried in an oven at 100 °C for 24 h.

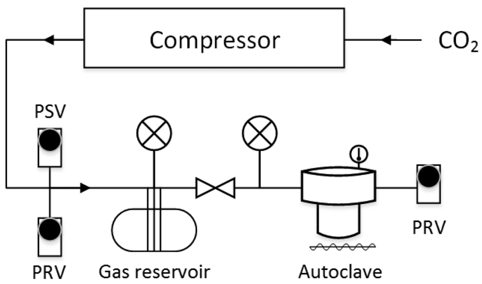

Figure 1. Mineral carbonation process flow diagram. The CO_2 pressure is generated by an air driven, double acting, reciprocating compressor ensuring a stable outlet flow. Compressed CO_2 is then pumped into the gas reservoir, and then continues through a manual valve and into the autoclave reaction chamber. The pressure inside the gas reservoir and the autoclave is regulated by the valve and pressure release valves (PRVs), and displayed by pressure gauges. An additional pressure safety valve is placed next to the gas reservoir, together with a drain valve (not indicated in figure). The reaction temperature is regulated using a cylindrical heater shaped to fit the autoclave while a magnetic stirrer ensures mixing.

Sample Characterization. Powder X-ray diffraction of dried products was measured on a Rigaku SmartLab diffractometer equipped with a Cu K_α source, parallel beam optics and a D/tex Ultra 1D detector. Powder patterns were analyzed by Rietveld refinement using the Fullprof software suite to obtain quantitative phase fractions of the final crystalline products.[33] Carbonation rates were calculated from the molar ratio between Mg_2SiO_4 and $MgCO_3$. A selected fully converted sample was heated in situ to 600 °C (in air) on the Rigaku diffractometer with an Anton Paar DHS 1100 domed hot stage equipped with a tungsten knife edge. SEM and EDX micrographs were obtained using a FEI NOVA SEM equipped with a TLD detector in secondary electron mode, and all images were taken under high vacuum. SEM, together with automated software, was used to determine size distributions for the two olivine samples.[34]

RESULTS & DISCUSSION

Olivine Size Distributions. Figure 2a, b shows the size distributions of the <10 μm and ~100 μm samples, whereas Figure 2c, d shows SEM images of the two samples. For the normal size distributions (red), particle areas were converted to a diameter equivalent to a spherical particle with the same area. Volume weighted distributions (blue) are also given together with the cumulative size distributions for both distributions. For the ~100 μm sample a flat distribution can be found centered at 100 μm together with a large peak at small diameters, corresponding to tiny grains that break of during handling of the sand. The large number of tiny grains shifts the mean particle size all the way down to around 50 μm. A better indicator of this distribution is the volume or mass distribution, resulting in a mean weight of 3.8 μg assuming a spherical particle with a diameter of 130 μm. From SEM images of the <10 μm sample, Figure 2c, a number of 2−10 μm particles are observed covered in a larger amount of smaller submicrometer

DOI: 10.1021/am508432w
ACS Appl. Mater. Interfaces 2015, 7, 5258−5264

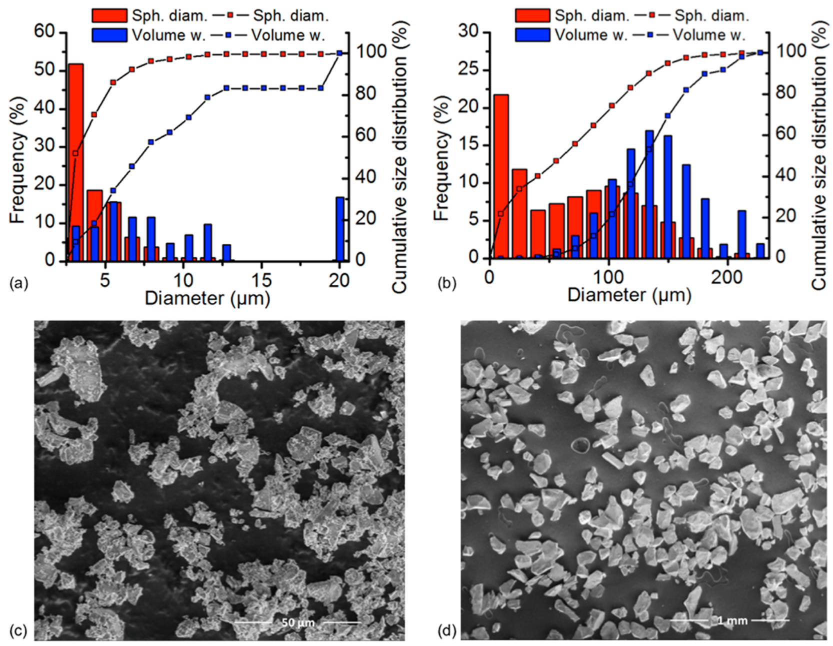

Figure 2. Size distribution for (a) the <10 μm sample and (b) the ~100 μm sample. The normal size distributions are given in red, whereas the volume or mass weighted distributions are given in blue. SEM images of (c) the <10 μm sample and (d) the ~100 μm sample.

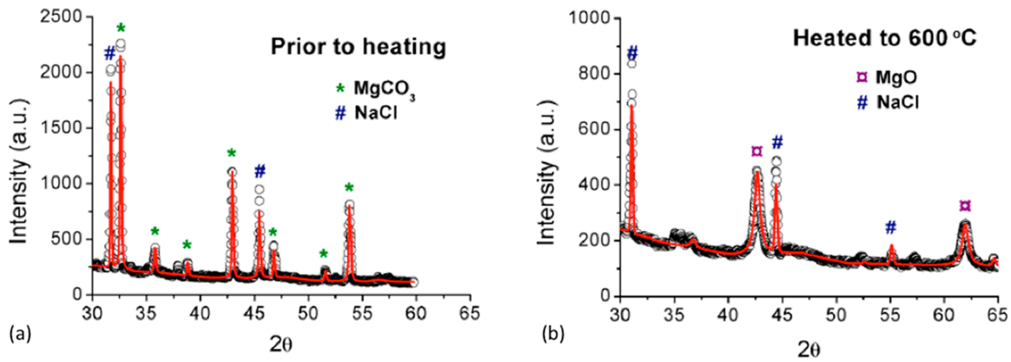

Figure 3. (a) Powder X-ray diffraction data from a fully converted olivine sample. Only crystalline phases of $MgCO_3$ and NaCl are present. (b) Rietveld refinement of PXRD pattern for the calcination product. PXRD patterns have been cut below 30° because of the presence of a large scattering signal from the carbon dome encasing the sample during heating.

sized particles. The automated software used was not able to include these submicrometer particles resulting in a cut off at 2.5 μm in the size distribution of the <10 μm sample. Although the large amounts of submicrometer sized particles are highly reactive, their contribution to the total mass of the sample is estimated to be less than a few percent. Using the mass weighted distribution, and accounting for the estimated submicrometer grain size contribution, the average weight of a grain is 0.0004 μg with a diameter of 6 μm.

Product Characterization, Calcination, and Amorphous Silica. Three distinct crystalline phases were observed in the PXRD diffractograms, namely $MgCO_3$, together with unreacted Mg_2SiO_4 and NaCl. No $NaHCO_3$ or Si-containing phases were observed. In Figure 3, a PXRD diffractogram of a fully converted sample is presented together with a sample heated to 600 °C (in air) in order to investigate the conversion from $MgCO_3$ to MgO during calcination. Profile analysis of the PXRD pattern suggests that the MgO powder has nanostructuring with individual crystalline particle sizes of around 12(3) nm determined by the Scherrer equation. Even after calcination of the product at 600 °C, no crystalline silica phases were observed. To confirm the formation of amorphous silica when carbonating olivine, SEM and simultaneously EDX measurements were performed on selected fully carbonated samples. In Figure 4, a representative SEM micrograph shows two clearly distinguishable phases, and the resulting relative

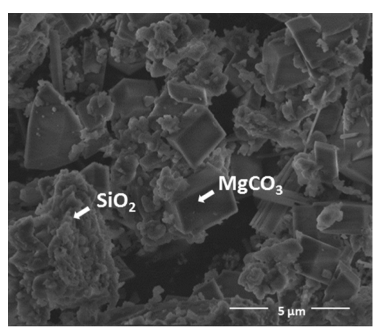

Figure 4. SEM image of a fully carbonated olivine sample. Energy-dispersive X-ray spectroscopy measurements reveal micrometer-sized $MgCO_3$ crystals and smaller amorphous silica particles.

DOI: 10.1021/am508432w
ACS Appl. Mater. Interfaces 2015, 7, 5258−5264

atomic percentages of different metals at the two measuring points are (Mg 65.2%, Ca 0.3%, Fe 5.9%, Si 16.1%, Al 7.1%, Na 5.4%) for the point centered on the large crystal, and (Mg 14.5%, Ca 0.1%, Fe 1.0%, Si 40.7%, Al 2.6%, Na 41.1%) for the point centered on small rounded particles. In an attempt to quantify the phases the following approximation is used: Mg, Ca and Fe originates from $Mg_{1-x}(Ca,Fe)_xCO_3$, Si and Al from the amorphous alumina silicate phases, and Na from NaCl. Under this assumption, the measuring point on the large crystal contains 71% $MgCO_3$, 23% silica, and 5% NaCl confirming that the micrometre sized crystals are $MgCO_3$. The significant amount of silica observed is most likely originating from the particles sticking to the crystal surface. The second measuring point contains 43% silica, 41% NaCl, and 16% $MgCO_3$ indicating that an amorphous silica phase is formed and that it sticks to the surface of the NaCl and $MgCO_3$ crystals. According to the work of Béarat et al., the formation of amorphous silica is thought to hinder CO_2 sequestration by covering the surface of olivine particles. Stirring the solution or adding abrasives can therefore increase carbonation yield by mechanically breaking the silica layers, exposing reactive olivine surface.[18] Additional information concerning the EDX measurements can be found in the Supporting Information.

Effect of Temperature and Particle Size on the Reaction Rate. On the basis of simple equilibrium thermodynamics, increasing the temperature from ambient conditions will lower the amount of dissolved CO_2 in the water phase (**2**), shift the carbonic acid equilibriums (**3**, **4**) toward the carbonate ion, and lower the solubility of $MgCO_3$ (**6**). Adding these different contributions together, a temperature increase of ∼100 °C should improve carbonation yield, even without accounting for kinetics.

In Figure 5, the conversion of <10 μm olivine particles at three different temperatures are plotted together with

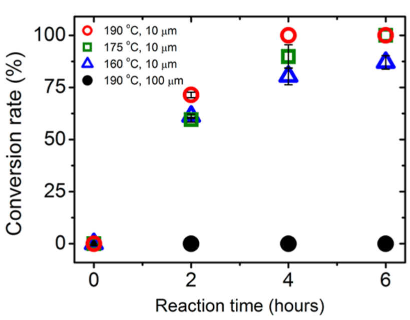

Figure 5. Conversion rate versus reaction time at different temperatures for the <10 μm olivine sample plotted (open symbols) together with conversion rates for the ∼100 μm sample at 190 °C (filled symbols). P_{CO2} = 100 bar, C_{NaHCO3} = 0.5 M, C_{NaCl} = 0.75 M.

conversion rates for the ∼100 μm olivine particles at the highest temperature of 190 °C. A substantial increase in conversion rates at higher temperatures was found for the <10 μm sized sample. At 190 °C, full conversion could be achieved within 4 h, whereas lowering the temperature 15° resulted in a conversion rate of 90%. Looking at the size effects, the liberation of Mg^{2+} is most likely to take place from the olivine surface.[35,36] The carbonation rate should therefore correlate with the available olivine surface area, leading to faster reactions for smaller particles. This was validated experimentally as small particles <10 μm could be readily converted, whereas larger particles of ∼100 μm could not be converted in the given time span of 6 h. This clearly indicates that olivine grains should be ground below a certain size before the carbonation reaction effectively can proceed to completion, under the present conditions.

Effect of pressure, $NaHCO_3$, and NaCl on the Reaction Rate. In contrast to temperature, higher CO_2 pressure increases the amount of dissolved carbonic acid (**2**) in the water phase. With no other acids in the solution, this will significantly lower the pH without any noticeable increase in the CO_3^{2-} concentration since to the equilibrium in equation (**4**) lies to the far left ($K_4 = 4.7 \times 10^{-11}$). Decreasing the pH is desirable since it contributes to the liberation of Mg^{2+} ions from olivine, although an extremely high Mg^{2+} concentration is needed to precipitate $MgCO_3$ because of the low carbonate ion concentration. To increase the CO_3^{2-} concentration, $NaHCO_3$ is added to the solution. Adding 0.5 M $NaHCO_3$ increases the carbonate ion concentration by more than 5 orders of magnitude and should therefore greatly enhance conversion rates because $MgCO_3$ will precipitate at a lower Mg^{2+} concentration.[32] Increasing the CO_2 pressure in a solution containing 0.5 M $NaHCO_3$ decreases the carbonate ion concentration by lowering the pH value, countering the pH increase from adding $NaHCO_3$. At p = 1 bar, T = 150 °C, and C_{NaHCO3} = 0.5 M $NaHCO_3$, the water solution has a pH value of 8.1, while raising the partial CO_2 pressure to 100 bar lowers the pH to around 6.1, based on equilibrium thermodynamic calculations.[32] In Figure 3a, conversion rates are plotted with varying concentration of $NaHCO_3$ while keeping a constant NaCl concentration and vice versa. The effect of pressure on the conversion rate is plotted in Figure 3b. Experimentally, $NaHCO_3$ addition greatly enhances the sequestration rate, with the carbonation yield jumping from below 5 to 100% upon increasing the $NaHCO_3$ concentration from 0 to 0.5 M. The CO_2 pressure is also found to have a big impact on the conversion rate, going from 22% conversion at 40 bar to complete conversion at 100 bar. Experimentally, the NaCl concentration was found to have minimal influence on the reaction rate, with a conversion rate of more than 90% in the absence of NaCl. In summary, to achieve efficient reaction rates, the olivine particles needs to be ground to a proper size well below 100 μm, the temperature increased to 190 °C, the pressure raised to 100 bar, and 0.5 M $NaHCO_3$ added to the solution. Under these conditions, olivine can readily be converted into $MgCO_3$ in less than 4 h with a yield of 100%. The simplicity of the studied reaction setup should enable a large scale CCS process.

Table 1. Overview of Previous Olivine Carbonation Studies

O'Connor[14,30] (2001, 2005), Gerdemann[17] (2007)	Investigation of olivine carbonation varying temperature and CO_2 pressure with the important addition of $NaHCO_3$ and NaCl as catalysts. Also include an economic and energy analysis.
McKelvy[37] (2006), Béarat[18] (2006)	Further study of the effect of high $NaHCO_3$ and $KHCO_3$ concentrations, including on bigger particles (<150 μm). Investigation of the role of the passivating amorphous silica layer, and attempts to counter its formation by adding quartz as abrasive.
Gadikota[28] (2014)	Focus on chemical and morphological changes during the reaction also with respect to $NaHCO_3$ and NaCl additives.

DOI: 10.1021/am508432w
ACS Appl. Mater. Interfaces 2015, 7, 5258−5264

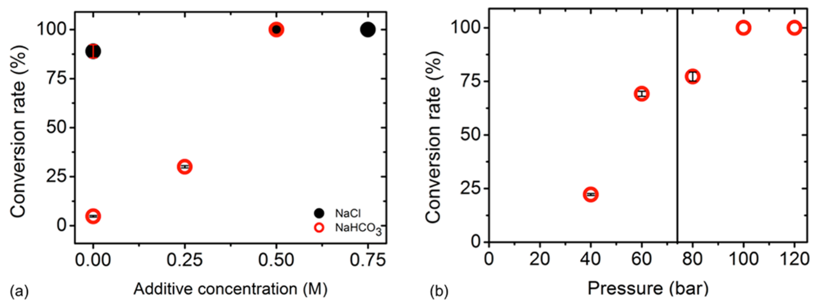

Figure 6. (a) Conversion rate versus additive concentration, P_{CO2} = 100 bar, T = 190 °C, particle size <10 μm, t = 4 h. Filled symbols indicate that the NaCl concentration is being varied at constant $NaHCO_3$ concentration (0.5 M), while the open symbols indicate a varying $NaHCO_3$ concentration at constant NaCl concentration (0.75 M). (b) Conversion rate dependence on applied pressure. T = 190 °C, particle <10 μm, t = 4 h, C_{NaHCO3} = 0.5 M, C_{NaCl} = 0.75 M. The black line indicates the transition to supercritical CO_2 (P_{crit} = 73 bar).

Comparison with Work by Others. An overview of previous, similar work is shown in Table 1. The temperature profile in Figure 5 agrees with the work of Gerdemann et al., who achieved optimal conversion rates around a temperature of 180 °C, followed by a decrease at higher temperatures, likely due to reduced CO_2 solubility.[17] Furthermore, their pressure profile exhibits a plateau in the conversion rate around the supercritical point of CO_2 (~73 bar), which is also observed in the present work, although here based on a single pressure point in Figure 6b. It would be interesting to study the implications of the phase transition in greater detail.

The result presented in Figure 6a shows that adding $NaHCO_3$ to the reaction is vital to achieve high conversion rates, even without the addition of NaCl. Addition of $NaHCO_3$ increases the carbonate concentration while steadily raising the pH of the solution. Because the leaching of Mg^{2+} ions from the olivine particle surface is more efficient at low pH values we would anticipate that the olivine carbonation rate will have a maximum at a certain $NaHCO_3$ concentration. This is observed in the work of McKelvy et al., where varying the $NaHCO_3$ concentration resulted in a broad carbonation maximum around 1.5−3.5 M, with almost no conversion at concentrations below 0.6 M, and low conversion rate above 3.5 M due to insufficient leaching of Mg^{2+}.[37] The data presented here on the other hand shows a conversion of more than 90% using a $NaHCO_3$ concentration of 0.5 M, without adding NaCl. This difference is most likely due to the difference in particle sizes with McKelvy et al. using bigger olivine particles with particle size <38 μm. In addition, they show that increasing the $NaHCO_3$ concentration to 2.5 M enhances the carbonation of bigger olivine particles (particle size <150 μm) to a greater extent than for the smaller particles (particle size <38 μm). Together with the results presented here, this indicates that the optimal $NaHCO_3$ concentration is highly dependent on the particle size, and that the maximum is shifted to lower $NaHCO_3$ concentrations for smaller particles. The low conversion rates for the ~100 μm sized particles are therefore most likely due to the relative low $NaHCO_3$ concentration. Another reason could be insufficient agitation of the slurry mixture caused by using bigger particles, although in this case we should have observed some amount of $MgCO_3$. The limited effect of adding NaCl was also found by Gadikota et al. using particles with a mean size of 21.4 μm, and can be accounted for by a slight pH lowering or reduction in the activity of water as the ionic strength of the solution is increased.[28] O'Connor et al. found, using bigger particles, that NaCl positively influence the conversion rate.[14] This indicates that higher ion concentration aids the conversion of bigger particles while having limited effect on smaller ones. McKelvy et al. also exchanged different amounts of Na^+ with the softer K^+ ion, resulting in lower yields.[37] This result cannot be explained by small pH changes, but may be explained by the decrease in ionic strength when exchanging Na^+ with K^+. Although the role of Na^+ and K^+ is not well understood, O'Connor et al. suggested that these cations may facilitate the ion exchange across the solid/liquid interphase by altering the surface charges of the magnesium silicate particles.[14] This reaction could be more important for the conversion of bigger particles, explaining why increased ionic strength seems to have a more significant effect on larger olivine particles.

CONCLUSION

The influence of experimental parameters on the conversion rate of Mg_2SiO_4 to $MgCO_3$ under hydrothermal conditions has been investigated. It was shown that full conversion could be achieved in less than 4 h, and that increased temperature had a positive effect on the extent of conversion. Particle size had a remarkable effect on the conversion rate suggesting that the initial Mg_2SiO_4 source should be ground to particle sizes well below 100 μm for effective conversion. Alternatively the $NaCHO_3$ concentration can be increased to carbonate larger particles. Overall the conversion rate was greatly enhanced by increased CO_2 pressure and the addition of $NaHCO_3$ whereas adding NaCl did not appear to have any significant influence when using <10 μm sized particles. By comparing the data presented here with earlier work, it has been found likely that the optimal additive concentration vary with the chosen olivine particle size with larger particles demanding higher concentrations. Further study of the correlation between optimal additive concentrations and particle size will likely increase the understanding of the different mechanisms during the carbonation reaction. SEM micrographs and EDX measurements revealed the formation of an amorphous silica phase along with micrometer-sized $MgCO_3$ particles. The relative simple setup for the carbonation of olivine presented here should enable a large-scale CCS process.

ASSOCIATED CONTENT

Supporting Information

Additional information concerning the size distribution calculations, EDX measurements, and PXRD data. This material is available free of charge via the Internet at http://pubs.acs.org/.

DOI: 10.1021/am508432w
ACS Appl. Mater. Interfaces 2015, 7, 5258−5264

■ AUTHOR INFORMATION

Corresponding Author

*E-mail: bo@chem.au.dk.

Notes

The authors declare no competing financial interest.

■ ACKNOWLEDGMENTS

The work was supported by the Danish National Research Foundation (DNRF93). P. Hald and J. Becker are thanked for help building the reactor setup. A.B.B. thanks the SINO Danish Center for funding.

■ REFERENCES

(1) Raupach, M. R.; Marland, G.; Ciais, P.; Quéré, P. L.; Canadell, J. G.; Klepper, G.; Field, C. B. Global and regional drivers of accelerating CO2 emissions. *Proc. Natl. Acad. Sci. U.S.A.* **2007**, *104*, 10288−10293.

(2) Lackner, K. S. A Guide to CO_2 Sequestration. *Science* **2003**, *300*, 1677−1678.

(3) Barker, D. J.; Turner, S. A.; Napier-Moore, P. A.; Clark, M.; Davison, J. E. CO_2 Capture in the Cement Industry. *Energy Proc.* **2009**, *1*, 87−94.

(4) Yu, K. M. K.; Curcic, I.; Gabriel, J.; Tsang, S. C. E. Recent Advances in CO_2 Capture and Utilization. *ChemSusChem* **2008**, *1*, 893−899.

(5) Wang, Q.; Luo, J.; Zhong, Z.; Borgna, A. CO_2 capture by solid adsorbents and their applications: current status and new trends. *Energy Environ. Sci.* **2011**, *4*, 42−55.

(6) Pan, S.-Y.; Chang, E. E.; Chiang, P.-C. CO_2 Capture by Accelerated Carbonation of Alkaline Wastes: A Review on Its Principles and Applications. *Aerosol Air Qual. Res.* **2012**, *12*, 770−791.

(7) Zevenhoven, R.; Fagerlund, J.; Songok, J. K. CO_2 Mineral Sequestration: Developments Toward Large-scale Application. *Greenhouse Gases: Sci. Technol.* **2011**, *1*, 48−57.

(8) Li, J.-R.; Kuppler, R. J.; Zhou, H.-C. Selective gas adsorption and separation in metal−organic frameworks. *Chem. Soc. Rev.* **2009**, *38*, 1477−1504.

(9) Dragea, T. C.; Kozynchenkob, O.; Pevidac, C.; Plazac, M. G.; Rubierac, F.; Pisc, J. J.; Snapea, C. E.; Tennisonb, S. Developing activated carbon adsorbents for pre-combustion CO_2 capture. *Energy Proc.* **2009**, *1*, 599−605.

(10) Montanari, T.; Busca, G. On the mechanism of adsorption and separation of CO_2 on LTA zeolites: An IR investigation. *Vib. Spectrosc.* **2008**, *46*, 45−51.

(11) Koukouzas, N.; Gemeni, V.; Ziock, H. J. Sequestration of CO_2 in Magnesium Silicates, in Western Macedonia, Greece. *Int. J. Miner. Process.* **2009**, *93*, 179−186.

(12) Fagerlund, J.; Nduagu, E.; Romão, I.; Zevenhoven, R. CO_2 Fixation Using Magnesium Silicate Minerals Part 1: Process Description and Performance. *Energy* **2012**, *41*, 184−191.

(13) Romão, I.; Nduagu, E.; Fagerlund, J.; Gando-Ferreira, L. M.; Zevenhoven, R. CO_2 Fixation Using Magnesium Silicate Minerals. Part 2: Energy Efficiency and Integration with Iron-and Steelmaking. *Energy* **2012**, *41*, 203−282.

(14) O'Connor, W. K.; Dahlin, D. C.; Rush, G. E.; Dahlin, C. L.; Collins, W. K. *Carbon Dioxide Sequestration by Direct Mineral Carbonation: Process Mineralogy of Feed and Products*; Report DOE/ARC-2001-027 ; National Energy Technology Laboratory, U.S. Department of Energy, Albany, NY, 2001.

(15) Zevenhoven, R.; Fagerlund, J.; Nduagu, E.; Romão, I.; Jie, B.; Highfield, J. Carbon Storage by Mineralisation (CSM): Serpentinite Rock Carbonation via $Mg(OH)_2$ Reaction Intermediate Without CO_2 Pre-separation. *Energy Procedia* **2013**, *37*, 5945−5954.

(16) Sipilä, J.; Teir, S.; Zevenhoven, R. Carbon Dioxide Sequestration by Mineral Carbonation Literature Review Update 2005−2007. Report, Åbo Akademi University, Åbo, Finland, 2008.

(17) Gerdemann, S. J.; O'Connor, W. K.; Dahlin, D. C.; Penner, L. R.; Rush, H. Ex Situ Aqueous Mineral Carbonation. *Environ. Sci. Technol.* **2007**, *41*, 2587−2593.

(18) Béarat, H.; McKelvy, M. J.; Chizmeshya, A. V. G.; Gormley, D.; Nunez, R.; Carpenter, R. W.; Squires, K.; Wolf, G. H. Carbon Sequestration via Aqueous Olivine Mineral Carbonation: Role of Passivating Layer Formation. *Environ. Sci. Technol.* **2006**, *40*, 4802−4808.

(19) Alexander, G.; Maroto-Valer, M. M.; Gafarova-Aksoy, P. Evaluation of Reaction Variables in the Dissolution of Serpentine for Mineral Carbonation. *Fuel* **2007**, *86*, 273−281.

(20) McKelvy, M. J.; Chizmeshya, A. V. G.; Diefenbacher, J.; Béarat, H.; Wolf, G. Exploration of the Role of Heat activation in Enhancing Serpentine Carbon Sequestration Reactions. *Environ. Sci. Technol.* **2004**, *38*, 6897−6903.

(21) Kelemen, P. B.; Matter, J.; Streit, E. E.; Rudge, J. F.; Curry, W. B.; Blusztajn, J. Rates and Mechanisms of Mineral Carbonation in Peridotite: Natural Processes and Recipes for Enhanced, In Situ CO_2 Capture and Storage. *Annu. Rev. Earth Planet. Sci.* **2011**, *39*, 545−576.

(22) Felmy, A. R.; Qafoku, O.; Arey, B. W.; Hu, J. Z.; Hu, M.; Schaef, H. T.; Ilton, E. S.; Hess, N. J.; Pearce, C. I.; Feng, J.; Rosso, K. M. Reaction of Water-saturated Supercritical CO_2 with Forsterite: Evidence for Magnesite Formation at Low Temperatures. *Geochim. Cosmochim. Acta* **2012**, *91*, 271−282.

(23) Lafay, R.; Montes-Hernandez, G.; Janots, E.; Chiriac, R.; Findling, N.; Toche, F. Simultaneous Precipitation of Magnesite and Lizardite from Hydrothermal Alteration of Olivine under High-carbonate Alkalinity. *Chem. Geol.* **2014**, *368*, 63−75.

(24) Fagerlund, J.; Teir, S.; Nduagu, E.; Zevenhoven, R. Carbonation of Magnesium Silicate Mineral Using a Pressurised Gas/Solid. Process. *Energy Proc.* **2009**, *1*, 4907−4914.

(25) Hänchen, M.; Prigiobbe, V.; Baciocchi, R.; Mazzotti, M. Precipitation in the Mg−carbonate System−Effects of Temperature and CO_2 Pressure. *Chem. Eng. Sci.* **2008**, *63*, 1012−1028.

(26) Huijgen, W. J. J.; Ruijg, G. J.; Comans, R. N. J.; Witkamp, G.-J. Energy Consumption and Net CO_2 Sequestration of Aqueous Mineral Carbonation. *Ind. Eng. Chem. Res.* **2006**, *45*, 9184−9194.

(27) Zevenhoven, R.; Fagerlund, J.; Nduagu, E.; Romão, I.; Jie, B.; Highfield, J. Carbon Storage by Mineralisation (CSM): Serpentinite Rock Carbonation via $Mg(OH)_2$ Reaction Intermediate Without CO_2 Pre-separation. *Energy Proc.* **2013**, *37*, 5945−5954.

(28) Gadikota, G.; Matter, J.; Kelemen, P.; Park, A.-h. A. Chemical and Morphological Changes During Olivine Carbonation for CO_2 Storage in the Presence of NaCl and $NaHCO_3$. *Phys. Chem. Chem. Phys.* **2014**, *16*, 4679−4693.

(29) Kwon, S.; Fan, M.; Dacosta, H. F. M.; Russell, A. G.; Tsouris, C. Reaction Kinetics of CO_2 Carbonation with Mg-Rich Minerals. *J. Phys. Chem. A* **2011**, *115*, 7638−7644.

(30) O'Connor, W. K.; Dahlin, D. C.; Rush, G. E.; Gerdemann, S. J.; Penner, L. R.; Nilsen, D. N.; *Aqueous Mineral Carbonation: Mineral Availability, Pretreatment, Reaction Parametrics, and Process Studies* ; Report DOE/ARC-TR-04-002 ; National Energy Technology Laboratory, U.S. Department of Energy: Albany, NY, 2005.

(31) Kwak, J. H.; Hu, J. Z.; Turcu, R. V. F.; Rosso, K. M.; Ilton, E. S.; Wang, C.; Sears, J. A.; Engelhard, M. H.; Felmy, A. R.; Hoyt, D. W. The Role of H_2O in the Carbonation of Forsterite in Supercritical CO_2. *Int. J. Greenhouse Gas Control* **2011**, *5*, 1081−1092.

(32) Chen, Z.-Y.; O'Connor, W. K.; Gerdemann, S. J. Chemistry of Aqueous Mineral Carbonation for Carbon Sequestration and Explanation of Experimental Results. *Environ. Prog.* **2006**, *25*, 161−166.

(33) Rodriguez-Carvajal, J. FULLPROF: A Program for Rietveld Refinement and Pattern Matching Analysis. Abstracts of the Satellite Meeting on Powder Diffraction of the XV Congress of the IUCr, Toulouse, France 1990.

(34) Schneider, C. A.; Rasband, W. S.; Eliceiri, K. W. NIH Image to ImageJ: 25 years of image analysis. *Nat. Methods* **2012**, *9*, 671−675.

(35) Hänchen, M.; Prigiobbe, V.; Storti, G.; Seward, T. M.; Mazzotti, M. Dissolution Kinetics of Fosteritic Olivine at 90−150 °C Including

Effects of the Presence of CO_2. *Geochim. Cosmochim. Acta* **2006**, *70*, 4403−4416.
(36) Penner, L. R.; Dahlin, D. C.; Gerdemann, S. J.; Saha, K. K. Modeling Flow of Mineralized Carbon Dioxide Slurry, 22nd Annual International Pittsburgh Coal Conference, Pittsburgh, 2005, *22*.
(37) McKelvy, M. J.; Chizmeshya, A. V. G.; Squires, K.; Carpenter, R. W.; Béarat, H. A Novel Approach To Mineral Carbonation: Enhancing Carbonation While Avoiding Mineral Pretreatment Process Cost. Technical Report, Arizona State University, Tucson, AZ, 2006.

DOI: 10.1021/am508432w
ACS Appl. Mater. Interfaces 2015, 7, 5258−5264